### Title

Human iPSC-Derived Immature Astroglia Promote Oligodendrogenesis by Increasing TIMP-1 Secretion




### Journal

Cell Reports, 15(6)

### ISSN

2639-1856



### Authors

Jiang, Peng
Chen, Chen
Liu, Xiao-Bo
et al.



### Publication Date

2016-05-01

### DOI

10.1016/j.celrep.2016.04.011

Peer reviewed

HHS Public Access

Author manuscript

*Cell Rep*. Author manuscript; available in PMC 2016 May 12.

Published in final edited form as:

*Cell Rep*. 2016 May 10; 15(6): 1303–1315. doi:10.1016/j.celrep.2016.04.011.

# Human iPSC-derived Immature Astroglia Promote Oligodendrogenesis by increased TIMP-1 Secretion

**Peng Jiang**[1,2,3,*], **Chen Chen**[2,3], **Xiao-Bo Liu**[2,4], **David E. Pleasure**[3,4], **Ying Liu**[6], and **Wenbin Deng**[2,3,4,*]

[1]Department of Developmental Neuroscience, Munroe-Meyer Institute; Holland Regenerative Medicine Program, University of Nebraska Medical Center, Omaha, NE 68198, USA

[2]Department of Biochemistry and Molecular Medicine, School of Medicine, University of California at Davis, Sacramento, CA 95817, USA

[3]Institute for Pediatric Regenerative Medicine, Shriners Hospitals for Children, Sacramento, CA 95817, USA

[4]Center for Neuroscience, School of Medicine, University of California at Davis, Davis, CA 95618, USA

[6]Department of Neurosurgery, University of Texas Health Science Center at Houston, Houston, TX 77030, USA

## SUMMARY

Astrocytes, once considered passive support cells, are increasingly appreciated as dynamic regulators of neuronal development and function, in part via secreted factors. The extent to which they similarly regulate oligodendrocytes, or proliferation and differentiation of oligodendrocyte progenitor cells (OPCs) is less well understood. Here, we generated astrocytes from human pluripotent stem cells (hiPSC-Astros) and demonstrate that immature astrocytes - as opposed to mature - promoted oligodendrogenesis in vitro. In the PVL mouse model of neonatal hypoxic/ischemic encephalopathy, associated with cerebral palsy in humans, transplanted immature hiPSC-Astros promote myelinogenesis and behavioral outcome. We further identified TIMP-1 as a selectively upregulated component secreted from immature hiPSC-Astros. Accordingly, in the rat PVL model, intranasal administration of conditioned medium from immature hiPSC-Astros promoted oligodendrocyte maturation in a TIMP-1 dependent manner. Our findings suggest stage-

[*]Address correspondence to: Dr. Peng Jiang (peng.jiang@unmc.edu) and Dr. Wenbin Deng (wbdeng@ucdavis.edu).

**Author Contributions**

PJ and WD designed experiments and interpreted data. PJ and CC carried out most of experiments with technical assistance from XL and YL. XL performed the electron microscopy analysis. YL performed the gene expression analysis. DEP provided critical input to the research design. WD directed the study. PJ and WD wrote the paper with input from all co-authors.

**Competing Financial Interests**

The authors declare no competing financial interests.

specific developmental interactions between astroglia and oligodendroglia, with important therapeutic implications for promoting myelinogenesis.

**Keywords**

human induced pluripotent stem cells; immature astrocytes; periventricular leukomalacia; oligodendrocytes; myelination

## INTRODUCTION

Astrocytes play important roles in organizing and maintaining brain structure and function (Barres, 2008). Astrocytes go through prenatal and protracted postnatal maturation during development and can undergo a spectrum of functional changes associated with development (Molofsky et al., 2012; Pekny and Pekna, 2014), serving stage-specific roles in assisting neuronal development, such as synapse stabilization and elimination (Chung et al., 2013; Molofsky et al., 2012). However, it is unclear how astrocytes, at specific immature and mature stages, may differently regulate development of oligodendrocytes, myelin-producing cells in the CNS.

Human pluripotent stem cells (hPSCs) including human embryonic stem cells (hESCs) and induced pluripotent stem cells (iPSCs) have been efficiently differentiated to astrocytes (Emdad et al., 2011; Jiang et al., 2013b; Krencik et al., 2011; Roybon et al., 2013; Shaltouki et al., 2013). The progenies differentiated from hPSCs are reflective of very early human development (< 6 weeks) (Patterson et al., 2012). Particularly, hPSC-derived astrocytes differentiated by using chemically defined, xeno-free protocols can be maintained at an immature stage in culture (Chen et al., 2014a; Emdad et al., 2011; Jiang et al., 2013b; Krencik et al., 2011; Shaltouki et al., 2013). Moreover, hPSC-derived immature astrocytes can be further differentiated to astrocytes with defined mature phenotypes (Krencik et al., 2011; Roybon et al., 2013). Thus, astroglia derived from hPSCs provides an unprecedented opportunity to investigate the interaction between oligodendroglia and human astrocytes that are at defined immature and mature stages.

Astrocytes are implicated to influence myelination in myelin loss disorders. Prior studies demonstrate that oligodendrocytes preferentially remyelinate axons in areas containing astrocytes (Franklin et al., 1991; Talbott et al., 2005). However, astroglia-based therapy for myelin loss disorders is less studied (Chen et al., 2015), because most of the disorders are associated with profound astrocyte activation and formation of glial scar (Pekny and Pekna, 2014). Scaring astrocytes are regarded as a barrier to regeneration, partly due to secretion of factors that halt survival and differentiation of oligodendroglia progenitor cells (OPCs) (Back et al., 2005; Nash et al., 2011). Recent studies also suggest that in acute phase of injuries, astrogliosis is a defensive reaction. Reactive astrocytes recapitulate numerous processes involved in early development of immature astroglia and exhibit positive effects in the acute phase of injuries (Pekny and Pekna, 2014), but reactivated processes often go awry later, turning on the detrimental effects of the astrocytes on regeneration (Gallo and Deneen, 2014). Recent studies (Jiang et al., 2013b; Noble et al., 2011) demonstrate that transplanted immature astrocytes do not become reactive after CNS injury. Immature but not mature

astrocytes are neuroprotective and suppress the activation of endogenous astrocytes and glial scar formation (Chen et al., 2015). Thus, there is a strong rationale to examine whether transplantation of hPSC-derived astrocytes at a defined immature stage could regulate differentiation of endogenous OPCs and promote myelinogenesis.

Perinatally acquired white matter injury, induced by perinatal hypoxia-ischemia and referred to as periventricular leukomalacia (PVL), is the most common cause of brain injury in premature infants. PVL is the leading cause of cerebral palsy and long-term neurological morbidity (Deng, 2010). Currently no effective treatment exists. One of major causes of the white matter injury is that pre-myelinating oligodendrocytes are particularly vulnerable in PVL (Haynes et al., 2003). The decrease of pre-myelinating oligodendrocytes leads to an upstream increase of OPCs, but these OPCs are arrested at the progenitor stage and fail to efficiently differentiate into myelin-producing oligodendrocytes (Fancy et al., 2011; Jablonska et al., 2012; Reid et al., 2012; Segovia et al., 2008). Here we report that immature hiPSC-derived astrocytes ("hiPSC-Astros"), but not mature hiPSC-Astros and mature astrocytes isolated from the human brain, strongly promote proliferation of OPCs and differentiation of OPCs to oligodendrocytes. Moreover, immature hiPSC-Astros promote myelination and recovery of behavioral performance in animal models of PVL injury. Mechanistically, we show that immature hiPSC-Astros regulate OPC differentiation via secreted molecules including tissue inhibitor of metalloproteinase-1 (TIMP-1) both *in vitro* and *in vivo*.

## RESULTS

### Generation of immature and mature hiPSC-Astros

By using our established protocol (Jiang et al., 2013b), we derived astroglia from two hiPSC lines generated from healthy individuals (Chen et al., 2014a) (Fig. S1A and B). These hiPSC-Astros expressed astroglial markers glial fibrillary acidic protein (GFAP) and S100β (Fig. S1C). We compared the regional identities of the hiPSC-Astros with human brain-derived astrocytes (hBrain-Astros) isolated from the cerebral cortex of human brain. Similar to hiPSC-Astros, hBrain-Astros expressed astroglial markers GFAP and S100β (Fig. 1A). We found that the hBrain-Astros mainly expressed the mid/forebrain marker OTX2 (Fig. 1B and G) but not the hindbrain/spinal cord-specific marker HOXB4 (Fig. 1C and G). There were nearly no hBrain-Astros expressing the ventral marker NKX2.1 (< 0.1%, Fig. 1D and G). Similarly, the vast majority of the hiPSC-Astros also showed mid/forebrain identity, as indicated by expressing OTX2 (Fig. 1B and G), but not HOXB4 (< 0.1%, Fig. 1C and G). A small percent of hiPSC-Astros weakly expressed NKX2.1 (Fig. 1C and G).

Nearly all the hiPSC-Astros also expressed human CD44 (hCD44) and vimentin (Fig. S1D), suggesting that these hiPSC-Astros were immature (Liu et al., 2004) (Dahl et al., 1981; Jiang et al., 2013b). We then induced immature hiPSC-Astros to become mature astrocytes by the treatment of fibroblast growth factor 1 (FGF1), leukemia inhibitory factor (LIF) and ciliary neurotrophic factor (CNTF) (Krencik et al., 2011; Roybon et al., 2013). After 30 to 50-day treatment, we first examined expression of an astroglial maturation marker, nuclear factor-1A (NF1A) (Deneen et al., 2006; Roybon et al., 2013), in order to verify the mature phenotypes of these human astrocytes. The expression of NF1A was abundant in the

immature hiPSC-Astros, but markedly reduced in the hBrain-Astros and mature hiPSC-Astros (Fig. 1E). Quantitative PCR results showed that the immature hiPSC-Astros had a significantly higher (3 fold) expression level of NF1A than hBrain-Astros and mature hiPSC-Astros (Fig. 1H). We further examined the expression of hCD44 and vimentin in these human astrocytes. Nearly all the hiPSC-Astros, hBrain-Astros and mature hiPSC-Astros were positive for hCD44 and vimentin staining (Fig. 1F). However, qPCR results indicated a significantly higher expression level of hCD44 in the immature hiPSC-Astros, compared to hBrain-Astros (1.7 fold) and mature hiPSC-Astros (2.6 fold) (Fig. 1H). Moreover, qPCR results also showed that immature hiPSC-Astro expressed the highest level of vimentin, which was 2.2 fold and 5.3 fold higher than hBrain-Astros and mature hiPSC-Astros, respectively (Fig. 1H). The expression levels of hCD44 and vimentin were higher in hBrain-Astros than those in mature hiPSC-Astros (Fig. 1H). We further observed that in the human brain tissues derived from normal patients at the age of less than 6 months, human immature astrocytes *in situ* labeled by GFAP or S100β also expressed hCD44 and vimentin (Fig. S1E and F).

We next quantified expression of mRNAs encoding the astrocyte-specific glutamate transporters excitatory amino acid transporter 1 and 2 (EAAT1 and 2) in all the astroglial preparations. Consistent with the previous study (Roybon et al., 2013), we found that EAAT1 was expressed at a higher level in mature hiPSC-Astros (1.9 fold) and hBrain-Astros (2.3 fold) than in immature hiPSC-Astros (Fig. 1I), while EAAT2 level was not significantly different. The hBrain-Astros expressed EAAT1 and 2 at levels similar to mature hiPSC-Astros. In agreement with the expression of glutamate transporters, hBrain-Astros and mature hiPSC-Astros had 1.6-fold increase in sodium-dependent glutamate transport activity, compared to immature hiPSC-Astros (Fig. 1J). In addition, it is generally accepted that mature astrocytes are not proliferative. We also observed significantly lower proliferation rate of mature hiPSC-Astros and hBrain-Astros than that of immature hiPSC-Astros (Fig. 1K). Together, these data demonstrate that the hiPSC-Astros in this study represent human astrocytes with immature phenotypes, whereas hBrain-Astros and the hiPSC-Astros treated with FGF1 represent human astrocytes with mature phenotypes.

## Immature hiPSC-Astros promote proliferation of OPCs

To develop astroglia-based cell therapy for myelin loss disorders, we first investigated how the astroglia differentiated from hiPSCs interact with oligodendroglia, particularly in the presence of neurons. To this end, we fed primary mixed neuron/glia culture at 7 days *in vitro* (DIV) with astrocyte-conditioned medium (ACM) collected from immature hiPSC-Astros (hiPSC-Astro ACM), from hBrain-Astros (hBrain-Astro ACM) or from mature hiPSC-Astro (mature hiPSC-Astro ACM). We then examined the population of oligodendroglial lineage cells in the culture at DIV 14 (Fig. 2A). At DIV 7, there were βIIITubulin$^+$ neurons, GFAP$^+$ astrocytes and OPCs labeled by NG2$^+$, platelet-derived growth factor receptor alpha (PDGFRα), or Olig2, but no MBP$^+$ mature oligodendrocytes (Fig. 2B). At DIV 14, oligodendroglial lineage cells identified by Olig2 staining were found in control group (Fig. 2C and E), but few of them were proliferating as indicated by not expressing Ki67 (Fig. 2C and E). Compared to control group, more Olig2$^+$ cells and Olig2$^+$/Ki67$^+$ proliferating cells were identified in the group treated with mature hiPSC-Astro ACM and in the group treated

with hBrain-Astro ACM (Fig. 2C and E). Notably, compared to mature hiPSC-Astro ACM and hBrain-Astro ACM groups, the group treated with hiPSC-Astro ACM had much more $Olig2^+$ cells and $Olig2^+/Ki67^+$ proliferating cells (Fig. 2C and E). For all the groups, the vast majority (> 93.0%) of the $Olig2^+$ cells were labeled by PDGFRα, indicating their nature of OPCs (Fig. 2D and F). Hence, human astrocytes promote proliferation of endogenous OPCs in the primary culture. Immature hiPSC-Astros have much stronger capacity in promoting OPC proliferation than mature hiPSC-Astros and hBrain-Astros.

### Immature hiPSC-Astros boost differentiation of OPCs to oligodendrocytes

We next examined the population of $MBP^+$ mature oligodendrocytes at 14 days (DIV 21) after addition of ACM (Fig. 3A). We used Olig1 to label the oligodendroglial cells in the cultures, because Olig2 expression might down-regulate as the OPCs initiate the myelination program (Jiang et al., 2013a). We found that in control group, there were few $MBP^+$ cells (Fig. 3B and D), and the majority of $Olig1^+$ oligodendroglia expressed PDGFRα (Fig. 3C), indicating that OPCs in control culture did not robustly differentiate to oligodendrocytes and were stuck in the progenitor cell stage. Compared to the control group, there were more $MBP^+$ cells in the mature hiPSC-Astro ACM and hBrain-Astro ACM groups. Strikingly, large numbers of $MBP^+$ oligodendrocytes were found in hiPSC-Astro ACM group, suggesting that hiPSC-Astro ACM promoted differentiation of OPCs to oligodendrocytes. Our previous study (Jiang et al., 2013b) reported the generation of two subtypes of human astrocytes from hESCs, NPC-Astros and Olig2PC-Astros. We observed that ACM collected from both of these two subtypes of hESC-derived immature astrocytes also strongly promoted OPC differentiation at DIV 21 (Fig. S2), indicating that the effects on OPC differentiation were common to all the immature astrocytes derived from hiPSCs and hESCs.

To examine the population of OPCs in the culture at DIV 21, we double stained Olig1 with PDGFRα. As expected, we found that there were significantly more $Olig1^+$ oligodendroglia in hiPSC-Astro ACM group (Fig. 3C and D), compared to control group, mature hiPSC-Astro ACM group and hBrain-Astro ACM group. Moreover, significantly more $Olig1^+/PDGFR\alpha^+$ OPCs were found in hiPSC-Astro ACM group (Fig. 3C and D) than in control group, mature hiPSC-Astro ACM group and hBrain-Astro ACM group. To further confirm these findings, we did qPCR to examine the gene expression of *Olig1*, mature oligodendroglial markers *Mbp*, *Plp*, and *Cnp*, and OPC marker *Pdgfra*. We consistently observed that hiPSC-Astro ACM group had the highest expression of *Olig1* (Fig. 3E). Gene transcripts encoding mature oligodendrocyte markers were also highly expressed in hiPSC-Astro ACM group. In particular, *Mbp* expression was 16.6 fold higher in hiPSC-Astro ACM group than that in control group. The expression *Plp* and *Cnp* was respectively 9.2 fold and 2.1 fold higher in hiPSC-Astro ACM group than those in control group. The expression of *Pdgfra* was lower (0.5 fold) in mature hiPSC-Astro ACM and hBrain-Astro ACM groups, compared to control and hiPSC-Astro ACM groups. Altogether, these data indicate that compared to the addition of mature hiPSC-Astro ACM or hBrain-Astros ACM, the addition of hiPSC-Astro ACM not only replenishes the OPCs pool by robustly promoting OPC proliferation, but also strongly boosts the differentiation of OPCs to oligodendrocytes.

### Immature hiPSC-Astros regulate OPC differentiation partly via release of TIMP-1

To explore the possible mechanisms underlying the effects of immature hiPSC-Astros on OPCs, we added the hiPSC-Astro ACM to purified culture of primary mouse OPCs, and found that hiPSC-Astro ACM similarly promoted proliferation and differentiation of OPCs in the purified culture (Fig. S3), suggesting that hiPSC-Astro ACM had direct effects on OPCs. Then, we performed global gene expression microarray and analyzed the data obtained from hiPSC1-Astros, hiPSC2-Astros and hESC-derived astrocytes, including NPC-Astros and Olig2PC-Astros (Chen et al., 2014a; Jiang et al., 2013b). We focused on analyzing the genes encoding astrocyte-secreted factors that were reported to directly regulate OPC proliferation and differentiation. The detailed information of these genes is shown in Table S1. Notably, immature astrocytes expressed gene transcripts encoding factors that both promote myelination, such as TIMP-1, laminin and TSPs (Fig. 4A), and inhibit myelination, such as CTGF, TnC and CXCL1 (Fig. 4B). Moreover, immature astrocytes expressed gene transcripts encoding PDGF and FGF2 (Fig. 4C), which are OPC mitogens. Therefore, the gene expression of secreted factors with various effects on OPCs may collectively account for the compositive effects of immature astrocytes on OPCs.

Among the gene transcripts encoding factors that promote myelination, we found that the top highly expressed gene was *TIMP-1*, which has been previously reported to critically regulate oligodendrocyte development in mice (Moore et al., 2011). We then verified the expression *of TIMP-1* in all human astrocytes by qPCR. The result showed that *TIMP-1* expression was abundant in immature hiPSC-Astros and hESC-Astros (Fig. 4D), whereas its expression was significantly decreased in mature hiPSC-Astros, mature hESC-Astros and hBrain-Astros (Fig. 4D). To further investigate the role *TIMP-1* in the effects of immature hiPSC-Astros on OPC differentiation, we inhibited *TIMP-1* expression in hiPSC-Astros by small interfering RNA (siRNA). qPCR analysis showed that, at 48 h after transfection of *TIMP-1* siRNA, *TIMP-1* expression was significantly reduced (5.8 fold), compared to hiPSC-Astros transfected with control siRNA (Fig. 4E). Next, we fed the primary mixed neuron/glia culture at DIV7 with conditioned medium collected from hiPSC-Astros transfected with *TIMP-1* siRNA (TIMP-1$^{siRNA}$ ACM), control conditioned medium collected from hiPSC-Astros transfected with control siRNA (Cont$^{siRNA}$ ACM), and TIMP-1$^{siRNA}$ ACM supplemented with TIMP-1 (10 ng/ml). Then, we examined OPC differentiation at DIV 21. There were less MBP$^{+}$ oligodendrocytes in TIMP-1$^{siRNA}$ ACM group than those in Cont$^{siRNA}$ ACM group (Fig. 4F and H). Adding TIMP-1 to TIMP-1$^{siRNA}$ ACM increased the percentage of MBP$^{+}$ oligodendrocytes. The total number of Olig1$^{+}$ cells was not significantly different among groups (Fig. 4G and H), suggesting that TIMP-1 knockdown did not change the effects on increasing OPC proliferation. We also observed that there were more Olig1$^{+}$/PDGFRα$^{+}$ OPCs in TIMP-1$^{siRNA}$ ACM group, compared to Cont$^{siRNA}$ and TIMP-1$^{siRNA}$ plus TIMP-1 ACM groups (Fig. 4G and H). Our qCPR results further confirmed these observations. *Olig1* expression was not significantly different among the three groups (Fig. 4I). TIMP-1$^{siRNA}$ ACM group had significantly lower expression of mature oligodendrocyte genes, *Mbp* (~ 0.5 fold), *Plp* (~0.5 fold) and *Cnp* (~0.6 fold), compared to Cont$^{siRNA}$ and TIMP-1$^{siRNA}$ plus TIMP-1 ACM groups. Together, these data indicate that TIMP-1 secreted by immature hiPSC-Astros contributes to their

effects on promoting OPC differentiation, but not to their effects on increasing OPC proliferation.

### Transplanted immature hiPSC-Astros promote myelination in a mouse model of PVL

Considering the effects of immature hiPSC-Astros on OPCs *in vitro*, we hypothesized that transplantation of immature hiPSC-Astros might promote myelination after PVL injury. To facilitate survival of transplanted cells, we induced insults in P6 *Rag1*−/− immunodeficient mice using unilateral carotid ligation followed with hypoxia, which resulted in selective injury to the subcortical white matter, without detectable injury to cortical neurons (Liu et al., 2011a; Shen et al., 2010). Consistent with our previous studies (Liu et al., 2011a; Shen et al., 2010), we observed reactive astrogliosis at 4 days after induction of PVL injury selectively in the ipsilateral side of the brain (Fig. S4A–C). The contralateral side of the brain was not significantly changed after PVL injury and was used as control. Due to the extremely low proliferation rate of mature hiPSC-Astros and hBrain-Astros (Fig. 1K) and low engraftment efficiency commonly seen from transplantation of terminally differentiated mature cells, it was technically difficult to collect ample mature human astrocytes and perform transplantation experiments with a good cell survival rate. Thus, we only transplanted immature hiPSC-Astros into the mouse brain at P7 when we started to see reactive astrocytes (Fig. 5A). Immature hiPSC-Astros were grafted to the periventricular area adjacent to the corpus callosum (CC) where hypo-myelination was observed (Liu et al., 2011a; Shen et al., 2010) (Fig. 5B). No tumor formation or overgrowth of transplanted cells was observed throughout the experiments. Transplanted hiPSC-Astros identified by human nuclei (hN) staining survived in the mouse brains at 4 days after transplantation (P11) (Fig. 5C). The majority of the transplanted cells were found located close to the hippocampus and the lateral ventricle. Similar to our previous transplantation studies (Jiang et al., 2013b), a small percentage of the hiPSC-Astros expressed GFAP *in vivo* at 4 days after transplantation, as indicated by the double-labeling of GFAP and hN (Fig. 5C, 9.2 ± 1.4% of the $hN^+$ cells were $GFAP^+$, n = 4). The transplanted cells did not differentiate to oligodendrocytes, as indicated by expressing hCD44 but lack of MBP and Olig2 (Fig. 5C and Fig. S4D). Next, we examined the number of oligodendroglial lineage cells in the CC. Consistent with previous studies (Jablonska et al., 2012; Reid et al., 2012; Segovia et al., 2008), in vehicle control group, the number of $Olig2^+$ oligodendroglia were increased in ipsilateral side, compared to contralateral side (Fig. 5D and E). Transplantation of hiPSC-Astros further increased the number of $Olig2^+$ cells in the CC of the ipsilateral side, but did not significantly affect the contralateral side (Fig. 5D and E). Similar to our previous studies (Liu et al., 2011a), we observed severe hypo-myelination selectively in the ipsilateral side at 4 days after PVL insult, as indicated by MBP staining (Fig. 5D and F). Quantification of fluorescence intensity of MBP staining revealed that there was higher MBP immuno-positivity in ipsilateral side in hiPSC-Astro group than those in vehicle control group (Fig. 5D and F). We further examined the number of immature and mature oligodendroglia, respectively identified by $Olig2^+/CC1^-$ and $Olig2^+/CC1^+$, in the ipsilateral sides of vehicle and hiPSC-Astro groups. There were significantly more immature and mature oligodendroglia cells in hiPSC-Astro group than in vehicle group (Fig. 5G). To further confirm that transplanted immature hiPSC-Astros promoted myelination, we examined the node of Ranvier and the density of myelinated axons in the ipsilateral side brains of the

vehicle and hiPSC-Astro groups. Consistently, there were more nodes of Ranvier, identified by β IV spectrin$^+$ staining flanked by Caspr$^+$ staining, in the hiPSC-Astro group, compared to vehicle group (Fig. S4E). Moreover, the electron microscopic analyses demonstrated that the density of myelinated axons in hiPSC-Astro group was significantly higher than that in vehicle group (Fig. S4F). In addition, the majority of transplanted hiPSC-Astros abundantly expressed TIMP-1 at this time point (Fig. 5H). We also transplanted immature TIMP-1$^{siRNA}$ hiPSC-Astros, in which TIMP-1 expression was inhibited. MBP immuno-positivity in ipsilateral sides at P11 in TIMP-1$^{siRNA}$ hiPSC-Astro and vehicle control groups was not significantly different (Fig. S4G), suggesting that TIMP-1 secreted by transplanted hiPSC-Astros crucially contribute to the maturation of endogenous OPCs.

## Transplanted immature hiPSC-Astros promote recovery of behavioral performance and myelination

To examine the behavioral performance of the animals, three groups of animals were used: sham group in which animals received sham PVL surgery and no vehicle PBS injection or cell transplantation, vehicle group in which animals received PVL surgery and PBS injection after the surgery, and hiPSC-Astro group in which animals received PVL surgery and hiPSC-Astro transplantation after the surgery. Consistent with our previous study, we observed no significant difference in motor functions in climbing on the wall with a slope angle of 45º (Liu et al., 2011a) from P11 to P21 among the three groups of animals. Myelin mass changes are highly associated with the higher functions of the brain (Liu et al., 2012). Accumulative studies have shown that myelination deficiency contributes to the development of long-term deficits in learning and memory in both mouse and rat models of PVL (Cengiz et al., 2011; Huang et al., 2009). We thus examined learning and memory ability of P60 adult mice in Morris water maze. All mice were able to swim normally and locate the hidden platform during training trials in Morris water maze test. As expected, mice in vehicle group had worse performance and required more time to find the platform than those in sham group. Analysis of escape latency revealed significant differences among sham, vehicle and hiPSC-Astro groups (Fig. 6A and C (1)–(3)). On navigation days 3 to 5, mice in sham group showed less escape latency compared to mice in vehicle group. Notably, on navigation day 4 and 5, mice in hiPSC-Astro group showed better performance compared to mice in vehicle group. In the probe trials, mice in sham and hiPSC-Astro groups showed better performance and spent significantly more time than vehicle group in the quadrant where the platform had been (Fig. 6B and C (4)–(6)). Moreover, we examined the distribution of transplanted hiPSC-Astros in the P60 animals. hN$^+$ cells were found close to the lateral ventricle and integrated into the hippocampus, close to the CA3 region (Fig. S5A). These transplanted cells maintained their astroglial lineage properties, as indicated by over half of them expressing GFAP (58.7 ± 3.4%, n = 7). However, at this time point, expression of TIMP-1 was undetectable in these transplanted hiPSC-Astros (Fig. S5B). We did not observe any abnormal cellular hypertrophy and massive proliferation of the vast majority of transplanted hiPSC-Astros, indicating that the transplanted hiPSC-Astro did not become reactive astrocytes.

Next, to further explore the differences in myelination that might contribute to the changes in behavioral performance, we first examined MBP expression in vehicle and hiPSC-Astro

groups at P60. We found that there was no significant difference in MBP immuno-positivity between contralateral and ipsilateral sides from both vehicle and hiPSC-Astro groups (Fig. S5C and D). Previous studies have demonstrated that cellular recovery in oligodendrocytes does not correlate with proper axonal myelination (Jablonska et al., 2012). We thus used electron microscopy to determine whether in our model, neonatal hypoxic-ischemic injury caused abnormalities in ultrastructure of myelinated axons at P60. We found that unmyelinated axons were distributed among myelinated axons in vehicle group (Fig. 6D and E). Compared to sham group, the density of myelinated axons in vehicle group was significantly lower (Fig. 6F). The density of myelinated axons in hiPSC-Astro group was similar to that in sham group and was significantly higher than that in vehicle group (Fig. 6F). Under higher magnification, some myelinated axons exhibited thinner myelin sheath in vehicle group, compared to sham and hiPSC-Astro groups (Fig. 6G). Scatter plot graph of g ratio analysis in Fig. 6H demonstrated that g ratio values from vehicle group were mostly between 0.8–0.9; however, g ratio values from sham and hiPSC-Astro groups were largely overlapped and were mostly between 0.7–0.8, with some being around 0.6. Notably, the majority of low caliber axons were unmyelinated in vehicle group (Fig. 6D) and thus many myelinated axons with large diameters were included for g ratio analysis (Fig. 6H). Compared to vehicle group, sham and hiPSC-Astro groups had significantly lower g ratio values (Fig. 6I). The effects of transplanted hiPSC-Astros on both the density of myelinated axons and g ratio may indicate their impact on axons, in addition to their impact on oligodendroglia myelination. Moreover, the significant but small differences in the density of myelinated axons among the groups may suggest that in all conditions, oligodendrocytes are able to mature into myelin-forming cells but the maturation is accelerated in sham and hiPSC-Astro groups, compared with vehicle group.

## Intranasal administration of immature hiPSC-Astro ACM promotes OPC maturation after PVL injury

To further compare the effects of immature and mature human astrocytes on OPC maturation after PVL injury and to investigate the role of TIMP-1, we intranasally applied the total concentrated factors collected from ACM. Similar to the mouse PVL model, unilateral carotid ligation followed by hypoxia (6% $O_2$ for 1 hr) in rats at P7 also resulted in selective white matter injury without evident injury to cortical neurons (Follett et al., 2000). Here we used the rat model of PVL to facilitate intranasal administration, because neonatal rats have more easily visible nares than neonatal mice. Starting from P8, we applied control (Cont) medium that had not been exposed to cells, concentrated mature hiPSC-Astro ACM, as well as $Cont^{siRNA}$ ACM and $TIMP\text{-}1^{siRNA}$ ACM, collected from immature hiPSC-Astros transfected with control and TIMP-1 siRNA, respectively (Fig. 7A). The ELISA assay confirmed the higher abundance of human TIMP-1 in $Cont^{siRNA}$ ACM than that in $TIMP\text{-}1^{siRNA}$ ACM or mature hiPSC-Astro ACM (Fig. S6A). The intranasal route allowed effective delivery directly to the brain from the nasal mucosa, as indicated by ELISA assay of the brain tissues collected at 1 hr after the last intranasal administration (Fig. S6B). At P11, we found that administration of both $Cont^{siRNA}$ and $TIMP\text{-}1^{siRNA}$ ACM significantly increased the number of $Olig2^{+}$ oligodendroglia not only in the ipsilateral side, but also in the contralateral side of the brain, compared to administration of Cont medium and mature hiPSC-Astro ACM (Fig. 7B and E). There were also more proliferating oligodendroglial

cells, identified by Ki67$^{+}$ and Olig2$^{+}$, in both ipsilateral and contralateral sides in Cont$^{siRNA}$ and TIMP-1$^{siRNA}$ ACM groups than those in Cont medium and mature iPSC-Astro ACM groups (Fig. 7B and F). MBP staining revealed that there was higher MBP immuno-positivity in ipsilateral side brain from Cont$^{siRNA}$ ACM group than in Cont medium group (Fig. 7C and G), indicating that ACM from immature hiPSC-Astro promoted OPC maturation. Administration of TIMP-1$^{siRNA}$ ACM or mature hiPSC-Astro ACM was not able to promote OPC maturation after PVL injury (Fig. 7C and G). Since there was an increased number of Olig2$^{+}$ cells but not MBP immuno-positivity in the ipsilateral side from TIMP-1$^{siRNA}$ ACM group, we further investigated whether these cells stayed at a progenitor stage. In the CC of the ipsilateral side, more Olig2$^{+}$ cells expressing OPC marker NG2 were found in TIMP-1$^{siRNA}$ ACM group than in Cont$^{siRNA}$ ACM group (Fig. 7D and H). Together, these results demonstrate that released factors such asTIMP-1, mediate the effects of immature hiPSC-Astros on promoting OPC maturation after PVL injury.

## DISCUSSION

By differentiating hPSCs to astrocytes with defined immature and mature phenotypes, we report a novel regulation of oligodendrocyte development by astrocytes at a previously understudied immature stage. We demonstrate that hiPSC-derived immature astroglial transplant or ACM promotes myelinogenesis and improves behavioral outcome in animal models of PVL. These results implicate a novel strategy for promoting myelinogenesis by hiPSC-derived immature astroglia.

Due to a lack of efficient methods for purifying and maintaining astrocytes with defined immature and mature phenotypes in culture (Foo et al., 2011), no specific studies have been performed to examine how astrocytes at specific developmental stages interact with oligodendrocytes. Krencik et al. (2011) show that hPSC-Astros become mature in a serum-free condition after a long period of time (180 days). Roybon et al. (2013) report that hPSC-Astros cultured in a serum-containing medium (1% fetal bovine serum) exhibit mature phenotypes after a short exposure to FGF1 (7 days). Here, we promote maturation of hiPSC-Astros in a serum-free medium containing FGF1. We find that after 30 to 50-day culture, immature hiPSC-Astros become mature as indicated by increased EAAT1 expression and glutamate uptake, and decreased expression of NF1A, hCD44 and vimentin, consistent with the observations of astrocyte maturation in human tissue (Bjorklund et al., 1984; Girgrah et al., 1991; Yamada et al., 1992). Moreover, immature and mature hiPSC-Astros also possess forebrain identity similar to hBrain-Astros. Thus, using our protocol, immature and mature human astrocytes could be efficiently derived from hPSCs, providing new opportunities to study human astrocyte development and developmental interactions between astroglia and oligodendroglia.

Our microarray gene analyses show that immature human astrocytes express gene transcripts encoding OPC mitogens and factors that inhibit OPC maturation to myelinating oligodendrocytes. We propose that the inhibitory factors and OPC mitogens work synergistically to promote OPC proliferation. Moreover, immature astrocytes express gene transcripts encoding factors that promote OPC maturation and myelination. By a combination of qPCR, siRNA knockdown and intranasal ACM administration experiments,

we provide both *in vitro* and *in vivo* evidence that TIMP-1 partially but critically mediates the effects of immature astrocytes on OPC differentiation, but not the effects on OPC proliferation. Hence, the effects of hiPSC-Astros on oligodendroglia could depend on which stage the oligodendroglia cells are at and which astrocyte-secreted factors the oligodendroglia cells are exposed to. The gene expression of secreted factors with multifaceted effects on OPCs may indicate finely regulatory effects of the immature astrocytes on oligodendroglial lineage progression. In addition, by analyzing a transcriptome database of mouse astrocytes (Cahoy et al., 2008), we consistently find that mouse immature astrocytes also express gene transcripts encoding factors that promote or inhibit myelination, and promote OPC proliferation (Fig. S7A–D). Interestingly, *Tgfb2*, encoding transforming growth factor β2 (TGFβ2), but not *Timp-1*, is prominently expressed in immature mouse astrocytes (Fig. S7B and E). Previous studies have demonstrated that TGFβ signaling pathway critically promotes oligodendrocyte differentiation (Palazuelos et al., 2014). Thus, it would be interesting to investigate whether immature human and mouse astrocytes regulate oligodendrocyte development through different mechanisms. The iPSC technology provides new opportunities to obtain human glial cells and to study their interactions. With further advancement and development in purification and separation of human astroglia and oligodendroglia (Sim et al., 2011), future studies are warranted to provide deep insights into human glial cell interactions.

Our *in vitro* findings indicate that immature hiPSC-Astros not only promote the OPC proliferation but also robustly boost OPC differentiation to oligodendrocytes. We further demonstrate that forebrain immature hiPSC-derived astroglial transplants rescue the hypo-myelination in a hypoxic/ischemic mouse model of PVL. We find that TIMP-1 expression is abundant in transplanted hiPSC-Astros at 4 days after transplantation and is undetectable at about 2 months after transplantation, which is consistent with our *in vitro* observation (Fig. 4D) and previously reported developmental regulation of TIMP-1 expression in astrocytes (Ulrich et al., 2005). Furthermore, our study of intranasal administration of $Cont^{siRNA}$ and $TIMP\text{-}1^{siRNA}$ ACM pinpoint the role of TIMP-1 in mediating the effects of ACM on promoting OPC differentiation *in vivo*. Taken together, through released factors such as TIMP-1, hiPSC-Astros promote myelination and behavioral recovery.

Intracerebral cell transplantation during the neonatal period is not ideal in clinical settings. We demonstrate that direct application of hiPSC-Astro ACM via intranasal administration promotes myelination after PVL injury. This study thus puts forward a notion of hiPSC-based cell-free therapy. It is tempting to suggest that this approach may be particularly useful in myelin disorders such as multiple sclerosis, where inflamed environment significantly compromises survival of transplanted cells. Administration of the cell-free, concentered factors that are released from human immature astrocytes may be effective in promoting remyelination (Chen et al., 2014b). Future secretomic studies may help identify more comprehensively all key factors released from hiPSC-Astros and further promote the translational potential of hiPSC-based cell-free therapy.

# EXPERIMENTAL PROCEDURES

## Culture of hiPSC

The two hiPSC lines, hiPSC1 and hiPSC2, were reprogrammed from healthy individuals' fibroblasts by using retroviruses encoding OCT4, SOX2, KLF4 and c-MYC (Fig. S1A) (Chen et al., 2014a). All experiments conducted on hPSCs adhered to approved Stem Cell Research Oversight Committee at University of California, Davis.

## Differentiation and culture of human astrocytes

Embryoid body-based differentiation procedure was used for astroglial differentiation of hiPSCs (Fig. S1B). The hBrain-Astros were isolated from the cerebral cortex of fetal human brain (ScienCell; Catalog number: 1800).

## Generation of astrocyte-conditioned medium

ACM was concentrated 50-fold using centrifugal concentrators (Millipore). Protein concentration was determined by BCA assay (Thermo Scientific) and ACM was fed to primary mixed neuron/glia culture at 100 μg/ml. TIMP-1$^{siRNA}$ ACM supplemented with TIMP-1 (10 ng/ml; Peprotech) was also fed to the primary culture.

## Immunostaining

Cells fixed with 4% paraformaldehyde and brain sections (18 μm thick) from P11–P60 mice and rats were processed for immunofluorescence staining (Liu et al., 2011b). The information for primary antibodies and dilutions were listed in Table S2. Images were captured using a Nikon Eclipse C1 or Nikon A1 confocal laser-scanning microscope.

## Microarray analysis and heat maps

Illumina bead array was performed for gene expression analysis (Liu et al., 2006). Array data were processed using Illumina GenomeStudio software (Illumina).

## PVL animal model

Animal experiments were performed following protocols approved by the Animal Care and Use Committees at the University of California, Davis. By unilateral carotid ligation (UCL) followed with hypoxia, we induced hypoxic/ischemic insults in P6 mouse pups of *Rag1*−/− immunodeficient mice (B6.129S7-*Rag1*$^{tm1Mom}$ on a C57BL/6 background, Jackson Lab) or P7 Long-Evans rat pups (Charles Rivers laboratories) (Follett et al., 2000).

## Cell transplantation

One day after induction of hypoxic/ischemic injury in mice (P7), cell transplantation was performed (Fig. 5A). Hamilton syringe and needle were used to deliver cells by inserting directed through the skull into the target site (Chen et al., 2014a).

### Intranasal administration

One day after induction of hypoxic/ischemic injury in rats, intranasal administration of concentrated ACM was performed (Fig. 7A). Control medium or ACM was administered every 12 h from P8 to P11.

### Electron microscopy

Brain tissues were fixed and sectioned as previously described (Jiang et al., 2013a). EM images were captured using a high resolution CCD camera (Gatan, Pleasanton, CA). Images were processed using DigitalMicrograph (Gatan). EM images were analyzed using ImageJ software.

### Morris water-maze test

The Morris water-maze test was performed with mice at P60 (Jiang et al., 2013b).

### Data analysis

For all experiments, analysis was derived from at least three independent experiments. All data are represented as mean ± s.e.m. The escape latency in the behavioral training tests was determined by two-way repeated measures analysis of variance (ANOVA). All other assessments were analyzed using Student's *t* test when only two groups were compared or one-way ANOVA when three or more groups were compared.

## Supplementary Material

Refer to Web version on PubMed Central for supplementary material.

## Acknowledgments

We thank Dr. Shenglan Li for assisting with gene expression analysis. This work was in part supported by grants from National Institutes of Health (R01NS061983, R01ES015988 and R01HD087566, to W.D.), the National Multiple Sclerosis Society (to W.D.) and Shriners Hospitals for Children (to W.D.). Y.L. was supported by California Institute of Regenerative Medicine (RT1-011071), the Memorial Hermann Foundation (Staman Ogilvie Fund) and the Bentsen Stroke Center. C.C. was supported by a postdoctoral fellowship from California Institute of Regenerative Medicine.

## References

Back SA, Tuohy TM, Chen H, Wallingford N, Craig A, Struve J, Luo NL, Banine F, Liu Y, Chang A, et al. Hyaluronan accumulates in demyelinated lesions and inhibits oligodendrocyte progenitor maturation. Nat Med. 2005; 11:966–972. [PubMed: 16086023]

Barres BA. The mystery and magic of glia: a perspective on their roles in health and disease. Neuron. 2008; 60:430–440. [PubMed: 18995817]

Bjorklund H, Eriksdotter-Nilsson M, Dahl D, Olson L. Astrocytes in smears of CNS tissues as visualized by GFA and vimentin immunofluorescence. Med Biol. 1984; 62:38–48. [PubMed: 6379328]

Cahoy JD, Emery B, Kaushal A, Foo LC, Zamanian JL, Christopherson KS, Xing Y, Lubischer JL, Krieg PA, Krupenko SA, et al. A transcriptome database for astrocytes, neurons, and oligodendrocytes: a new resource for understanding brain development and function. J Neurosci. 2008; 28:264–278. [PubMed: 18171944]

Cengiz P, Uluc K, Kendigelen P, Akture E, Hutchinson E, Song C, Zhang L, Lee J, Budoff GE, Meyerand E, et al. Chronic neurological deficits in mice after perinatal hypoxia and ischemia

correlate with hemispheric tissue loss and white matter injury detected by MRI. Dev Neurosci. 2011; 33:270–279. [PubMed: 21701150]

Chen C, Chan A, Wen H, Chung SH, Deng W, Jiang P. Stem and Progenitor Cell-Derived Astroglia Therapies for Neurological Diseases. Trends Mol Med. 2015; 21:715–729. [PubMed: 26443123]

Chen C, Jiang P, Xue H, Peterson SE, Tran HT, McCann AE, Parast MM, Li S, Pleasure DE, Laurent LC, et al. Role of astroglia in Down's syndrome revealed by patient-derived human-induced pluripotent stem cells. Nat Commun. 2014a; 5:4430. [PubMed: 25034944]

Chen L, Coleman R, Leang R, Tran H, Kopf A, Walsh CM, Sears-Kraxberger I, Steward O, Macklin WB, Loring JF, et al. Human neural precursor cells promote neurologic recovery in a viral model of multiple sclerosis. Stem Cell Rep. 2014b; 2:825–837.

Chung WS, Clarke LE, Wang GX, Stafford BK, Sher A, Chakraborty C, Joung J, Foo LC, Thompson A, Chen C, et al. Astrocytes mediate synapse elimination through MEGF10 and MERTK pathways. Nature. 2013; 504:394–400. [PubMed: 24270812]

Dahl D, Rueger DC, Bignami A, Weber K, Osborn M. Vimentin, the 57 000 molecular weight protein of fibroblast filaments, is the major cytoskeletal component in immature glia. Eur J Cell Biol. 1981; 24:191–196. [PubMed: 7285936]

Deneen B, Ho R, Lukaszewicz A, Hochstim CJ, Gronostajski RM, Anderson DJ. The transcription factor NFIA controls the onset of gliogenesis in the developing spinal cord. Neuron. 2006; 52:953–968. [PubMed: 17178400]

Deng W. Neurobiology of injury to the developing brain. Nat Rev Neurol. 2010; 6:328–336. [PubMed: 20479779]

Emdad L, D'Souza SL, Kothari HP, Qadeer ZA, Germano IM. Efficient differentiation of human embryonic and induced pluripotent stem cells into functional astrocytes. Stem Cells Dev. 2011; 21:404–410. [PubMed: 21631388]

Fancy SP, Harrington EP, Yuen TJ, Silbereis JC, Zhao C, Baranzini SE, Bruce CC, Otero JJ, Huang EJ, Nusse R, et al. Axin2 as regulatory and therapeutic target in newborn brain injury and remyelination. Nat Neurosci. 2011; 14:1009–1016. [PubMed: 21706018]

Follett PL, Rosenberg PA, Volpe JJ, Jensen FE. NBQX attenuates excitotoxic injury in developing white matter. J Neurosci. 2000; 20:9235–9241. [PubMed: 11125001]

Foo LC, Allen NJ, Bushong EA, Ventura PB, Chung WS, Zhou L, Cahoy JD, Daneman R, Zong H, Ellisman MH, et al. Development of a method for the purification and culture of rodent astrocytes. Neuron. 2011; 71:799–811. [PubMed: 21903074]

Franklin RJ, Crang AJ, Blakemore WF. Transplanted type-1 astrocytes facilitate repair of demyelinating lesions by host oligodendrocytes in adult rat spinal cord. J Neurocytol. 1991; 20:420–430. [PubMed: 1869880]

Gallo V, Deneen B. Glial development: the crossroads of regeneration and repair in the CNS. Neuron. 2014; 83:283–308. [PubMed: 25033178]

Girgrah N, Letarte M, Becker LE, Cruz TF, Theriault E, Moscarello MA. Localization of the CD44 glycoprotein to fibrous astrocytes in normal white matter and to reactive astrocytes in active lesions in multiple sclerosis. J Neuropathol Exp Neurol. 1991; 50:779–792. [PubMed: 1748883]

Haynes RL, Folkerth RD, Keefe RJ, Sung I, Swzeda LI, Rosenberg PA, Volpe JJ, Kinney HC. Nitrosative and oxidative injury to premyelinating oligodendrocytes in periventricular leukomalacia. J Neuropathol Exp Neurol. 2003; 62:441–450. [PubMed: 12769184]

Huang Z, Liu J, Cheung PY, Chen C. Long-term cognitive impairment and myelination deficiency in a rat model of perinatal hypoxic-ischemic brain injury. Brain Res. 2009; 1301:100–109. [PubMed: 19747899]

Jablonska B, Scafidi J, Aguirre A, Vaccarino F, Nguyen V, Borok E, Horvath TL, Rowitch DH, Gallo V. Oligodendrocyte regeneration after neonatal hypoxia requires FoxO1-mediated p27Kip1 expression. J Neurosci. 2012; 32:14775–14793. [PubMed: 23077062]

Jiang P, Chen C, Liu XB, Selvaraj V, Liu W, Feldman DH, Liu Y, Pleasure DE, Li RA, Deng W. Generation and characterization of spiking and nonspiking oligodendroglial progenitor cells from embryonic stem cells. Stem Cells. 2013a; 31:2620–2631. [PubMed: 23940003]

Jiang P, Chen C, Wang R, Chechneva OV, Chung SH, Rao MS, Pleasure DE, Liu Y, Zhang Q, Deng W. hESC-derived Olig2+ progenitors generate a subtype of astroglia with protective effects against ischaemic brain injury. Nat Commun. 2013b; 4:2196. [PubMed: 23880652]

Krencik R, Weick JP, Liu Y, Zhang ZJ, Zhang SC. Specification of transplantable astroglial subtypes from human pluripotent stem cells. Nat Biotechnol. 2011; 29:528–534. [PubMed: 21602806]

Liu J, Dietz K, DeLoyht JM, Pedre X, Kelkar D, Kaur J, Vialou V, Lobo MK, Dietz DM, Nestler EJ, et al. Impaired adult myelination in the prefrontal cortex of socially isolated mice. Nature Neurosci. 2012; 15:1621–1623. [PubMed: 23143512]

Liu W, Shen Y, Plane JM, Pleasure DE, Deng W. Neuroprotective potential of erythropoietin and its derivative carbamylated erythropoietin in periventricular leukomalacia. Exp Neurol. 2011a; 230:227–239. [PubMed: 21596035]

Liu Y, Han SS, Wu Y, Tuohy TM, Xue H, Cai J, Back SA, Sherman LS, Fischer I, Rao MS. CD44 expression identifies astrocyte-restricted precursor cells. Dev Biol. 2004; 276:31–46. [PubMed: 15531362]

Liu Y, Jiang P, Deng W. OLIG gene targeting in human pluripotent stem cells for motor neuron and oligodendrocyte differentiation. Nat Prot. 2011b; 6:640–655.

Liu Y, Shin S, Zeng X, Zhan M, Gonzalez R, Mueller FJ, Schwartz CM, Xue H, Li H, Baker SC, et al. Genome wide profiling of human embryonic stem cells (hESCs), their derivatives and embryonal carcinoma cells to develop base profiles of U.S. Federal government approved hESC lines. BMC Dev Biol. 2006; 6:20. [PubMed: 16672070]

Molofsky AV, Krencik R, Ullian EM, Tsai HH, Deneen B, Richardson WD, Barres BA, Rowitch DH. Astrocytes and disease: a neurodevelopmental perspective. Genes Dev. 2012; 26:891–907. [PubMed: 22549954]

Moore CS, Milner R, Nishiyama A, Frausto RF, Serwanski DR, Pagarigan RR, Whitton JL, Miller RH, Crocker SJ. Astrocytic tissue inhibitor of metalloproteinase-1 (TIMP-1) promotes oligodendrocyte differentiation and enhances CNS myelination. J Neurosci. 2011; 31:6247–6254. [PubMed: 21508247]

Nash B, Thomson CE, Linington C, Arthur AT, McClure JD, McBride MW, Barnett SC. Functional duality of astrocytes in myelination. J Neurosci. 2011; 31:13028–13038. [PubMed: 21917786]

Noble M, Davies JE, Mayer-Proschel M, Proschel C, Davies SJ. Precursor cell biology and the development of astrocyte transplantation therapies: lessons from spinal cord injury. Neurotherapeutics. 2011; 8:677–693. [PubMed: 21918888]

Palazuelos J, Klingener M, Aguirre A. TGFbeta signaling regulates the timing of CNS myelination by modulating oligodendrocyte progenitor cell cycle exit through SMAD3/4/FoxO1/Sp1. J Neurosci. 2014; 34:7917–7930. [PubMed: 24899714]

Patterson M, Chan DN, Ha I, Case D, Cui Y, Van Handel B, Mikkola HK, Lowry WE. Defining the nature of human pluripotent stem cell progeny. Cell Res. 2012; 22:178–193. [PubMed: 21844894]

Pekny M, Pekna M. Astrocyte Reactivity and Reactive Astrogliosis: Costs and Benefits. Physiol Rev. 2014; 94:1077–1098. [PubMed: 25287860]

Reid MV, Murray KA, Marsh ED, Golden JA, Simmons RA, Grinspan JB. Delayed myelination in an intrauterine growth retardation model is mediated by oxidative stress upregulating bone morphogenetic protein 4. J Neuropathol Exp Neurol. 2012; 71:640–653. [PubMed: 22710965]

Roybon L, Lamas NJ, Garcia-Diaz A, Yang EJ, Sattler R, Jackson-Lewis V, Kim YA, Kachel CA, Rothstein JD, Przedborski S, et al. Human stem cell-derived spinal cord astrocytes with defined mature or reactive phenotypes. Cell Rep. 2013; 4:1035–1048. [PubMed: 23994478]

Segovia KN, McClure M, Moravec M, Luo NL, Wan Y, Gong X, Riddle A, Craig A, Struve J, Sherman LS, et al. Arrested oligodendrocyte lineage maturation in chronic perinatal white matter injury. Annals Neurol. 2008; 63:520–530.

Shaltouki A, Peng J, Liu Q, Rao MS, Zeng X. Efficient Generation of Astrocytes From Human Pluripotent Stem Cells in Defined Conditions. Stem Cells. 2013; 31:941–952. [PubMed: 23341249]

Shen Y, Plane JM, Deng W. Mouse models of periventricular leukomalacia. J Vis Exp. 2010; 39 pii: 1951. http://www.jove.com/index/Details.stp?ID=1951. 10.3791/1951

Sim FJ, McClain CR, Schanz SJ, Protack TL, Windrem MS, Goldman SA. CD140a identifies a population of highly myelinogenic, migration-competent and efficiently engrafting human oligodendrocyte progenitor cells. Nat Biotechnol. 2011; 29:934–941. [PubMed: 21947029]

Talbott JF, Loy DN, Liu Y, Qiu MS, Bunge MB, Rao MS, Whittemore SR. Endogenous Nkx2.2+/Olig2+ oligodendrocyte precursor cells fail to remyelinate the demyelinated adult rat spinal cord in the absence of astrocytes. Exp Neurol. 2005; 192:11–24. [PubMed: 15698615]

Ulrich R, Gerhauser I, Seeliger F, Baumgartner W, Alldinger S. Matrix metalloproteinases and their inhibitors in the developing mouse brain and spinal cord: a reverse transcription quantitative polymerase chain reaction study. Dev Neurosci. 2005; 27:408–418. [PubMed: 16280637]

Yamada T, Kawamata T, Walker DG, McGeer PL. Vimentin immunoreactivity in normal and pathological human brain tissue. Acta Neuropathologica. 1992; 84:157–162. [PubMed: 1523971]

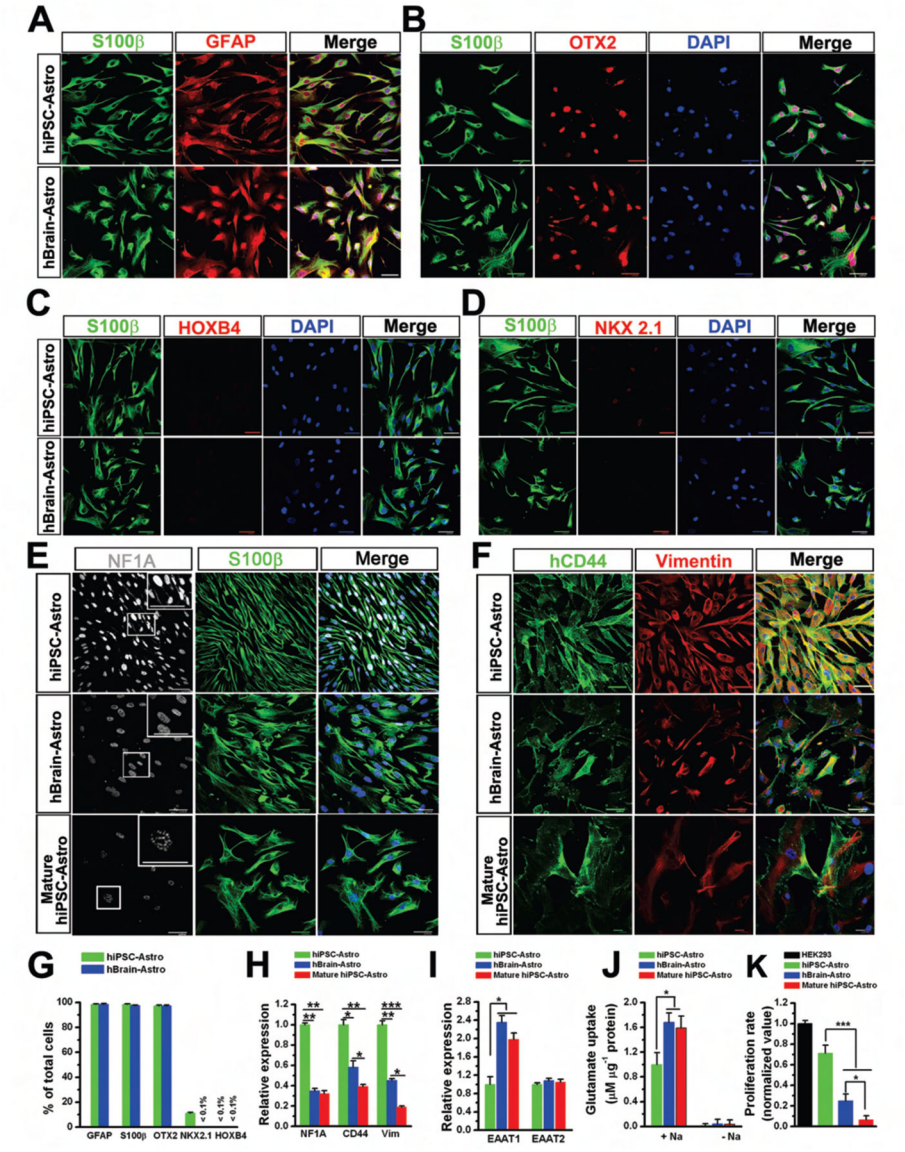


**Figure 1. Differentiation of hiPSC-Astros to human astrocytes with mature phenotypes**

**(A)** Representatives of GFAP$^+$ and S100β$^+$ hiPSC-Astros and hBrain-Astros.

**(B–D)** Representatives of OTX2- (B), HOXB4- (C) and NKX2.1-expressing cells (D) in the S100β$^+$ hiPSC-Astros and hBrain-Astros.

**(E)** Representative images showing that expression of NF1A is abundant in immature hiPSC-Astros, but markedly reduced in mature hiPSC-Astros and hBrain-Astros. Insets, enlarged images from the squared areas.

**(F)** Representatives of hCD44- and vimentin-expressing cells in hiPSC-Astros, hBrain-Astros and mature hiPSC-Astros.

**(G)** The percentage of GFAP-, S100β-, OTX2-, HOXB4- and NKX2.1-expressing cells in hiPSC-Astros and hBrain-Astros (n = 4 for each cell line). All quantitative data for hiPSC-Astros are analyses of pooled data collected from hiPSC1-Astros and hiPSC2-Astros.

**(H)** qPCR analysis of NF1A, hCD44 and vimentin (Vim) mRNA expression in the three groups of human astrocytes (n = 4 from each cell line). One-way ANOVA test, *P < 0.05, **P < 0.01 and ***P < 0.001.

**(I)** qPCR analysis of EAAT1 and 2 mRNA expression in the three groups of human astrocytes (n = 4 from each cell line). One-way ANOVA test, *P < 0.05.

**(J)** Glutamate uptake analysis showing that mature hiPSC-Astros and hBrain-Astros exhibit glutamate uptake at a higher rate than immature hiPSC-Astros (n = 4 from each cell line). This uptake capability is $Na^+$-dependent and can be abolished by the $Na^+$-free solution. One-way ANOVA test, *P < 0.05.

**(K)** Proliferation rate of the three groups of human astrocytes relative to HEK293 cells (n = 4 from each cell line). One-way ANOVA test, * P < 0.05 and ***P < 0.001. Scale bars, 50 μm. Blue, DAPI-stained nuclei.

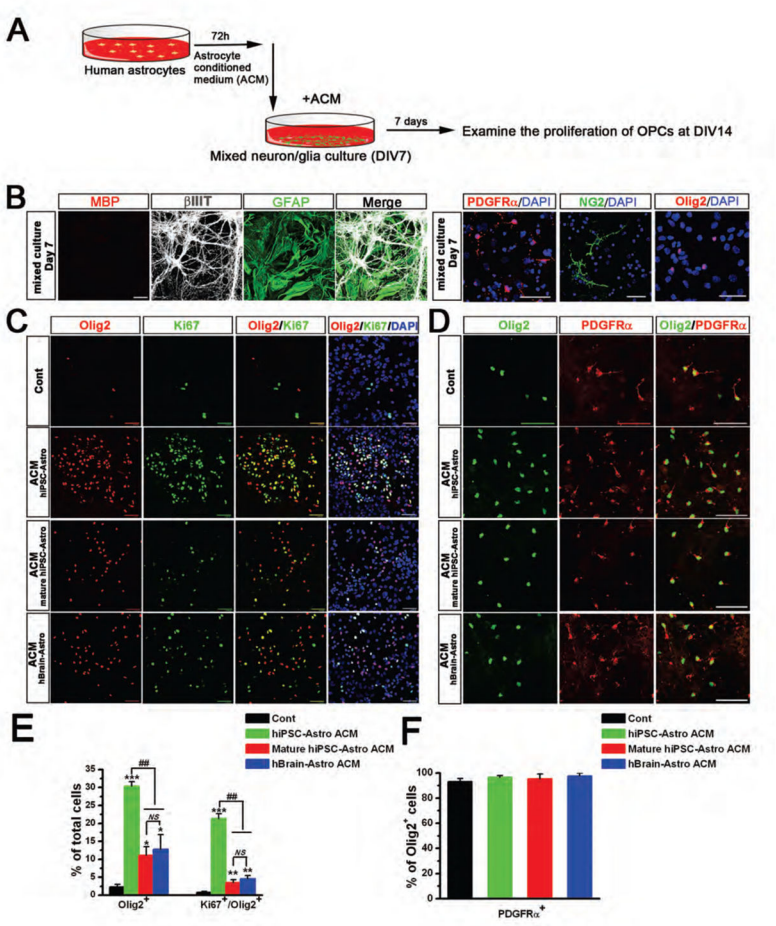


**Figure 2. The effects of immature and mature human astrocytes on OPC proliferation**

**(A)** A schematic diagram showing that the primary mixed neuron/glia culture at DIV 7 were treated with ACM and the proliferation of OPCs is examined 7 days after treatment of ACM (DIV 14).

**(B)** Representatives of βIII-tubulin $(\beta IIIT)^+$ neurons, $GFAP^+$ astrocytes, and OPCs labeled by PDGFRα, NG2 and Olig2 in the mixed culture at DIV 7. There is no $MBP^+$ oligodendrocyte in the culture.

**(C)** Representatives of $Olig2^+$ oligodendroglial lineage cells and $Ki67^+$ proliferating cells in the control (Cont) culture and cultures fed with hiPSC-Astro ACM, mature hiPSC-Astro ACM and hBrain-Astro ACM.

**(D)** Representatives of $Olig2^+$ and $PDGFR\alpha^+$ in the cultures fed with the different ACM.

**(E)** The percentage of $Olig2^+$ and $Ki67^+/Olig2^+$ cells in the cultures fed with the different ACM (n = 3 from each cell line). All the quantitative data for hiPSC-Astros and mature hiPSC-Astros are analyses of pooled data collected from hiPSC1-Astros and hiPSC2-Astros, and mature hiPSC1-Astros and hiPSC2-Astros, respectively. One-way ANOVA test, $^*P < 0.05$, $^{**}P < 0.01$, and $^{***}P < 0.001$, comparison between control group versus the groups treated with the different ACM; $^{\#\#}P < 0.01$; and *NS*, not significant.

**(F)** Quantification of the percentage of $PDGFR\alpha^+$ cells in total $Olig2^+$ cells (n = 3 from each cell line). One-way ANOVA test, $P > 0.05$. Scale bars, 50 μm.

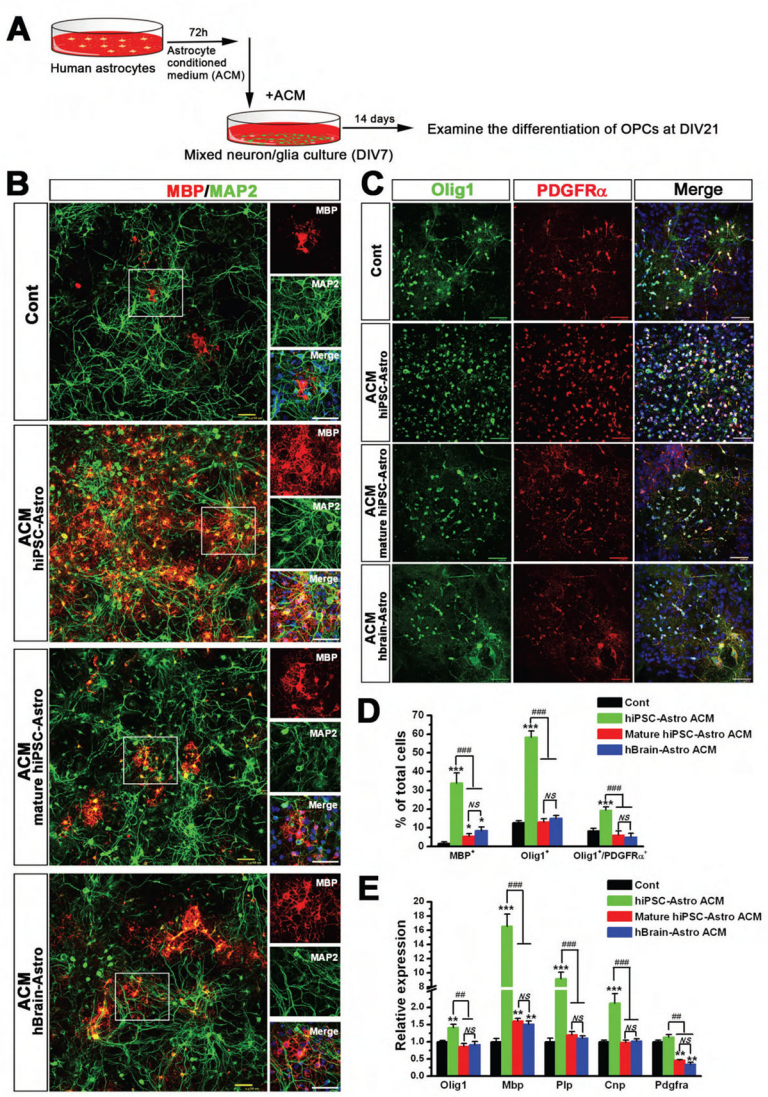


**Figure 3. The effects of immature and mature human astrocytes on OPC differentiation**

**(A)** A schematic diagram showing that the differentiation of OPCs to oligodendrocytes in the primary mixed neuron/glia culture is examined after 14-day treatment of ACM (DIV 21).

**(B)** Representatives of $MBP^+$ oligodendrocytes and $MAP2^+$ neurons in Cont culture and the cultures fed with hiPSC-Astro ACM, mature hiPSC-Astro ACM and hBrain-Astro ACM. The squared areas are enlarged.

**(C)** Representatives of $Olig1^+$ oligodendroglial lineage cells and $PDGFR\alpha^+$ OPCs in the mix cultures fed with the different ACM.

**(D)** Quantification of pooled data showing the percentage of $MBP^+$, $Olig1^+$ and $Olig1^+/PDGFR\alpha^+$ cells in the cultures fed with the different ACM (n = 3 from each cell line). One-way ANOVA test, *P < 0.05 and ***P < 0.001, comparison between control group versus the groups treated with the different ACM; $^{###}P < 0.001$; and *NS,* not significant.

**(E)** qPCR analysis of *Olig1, Mbp, Plp, Cnp* and *Pdgfra* expression in the cultures fed with the different ACM (n = 3 from each cell line). One-way ANOVA test, **P < 0.01 and ***P

< 0.001, comparison between control group versus the groups treated with the different ACM; ##P < 0.01 and ###P < 0.001 and *NS,* not significant. Scale bars, 50 μm in the original and enlarged images. Blue, DAPI-stained nuclei.

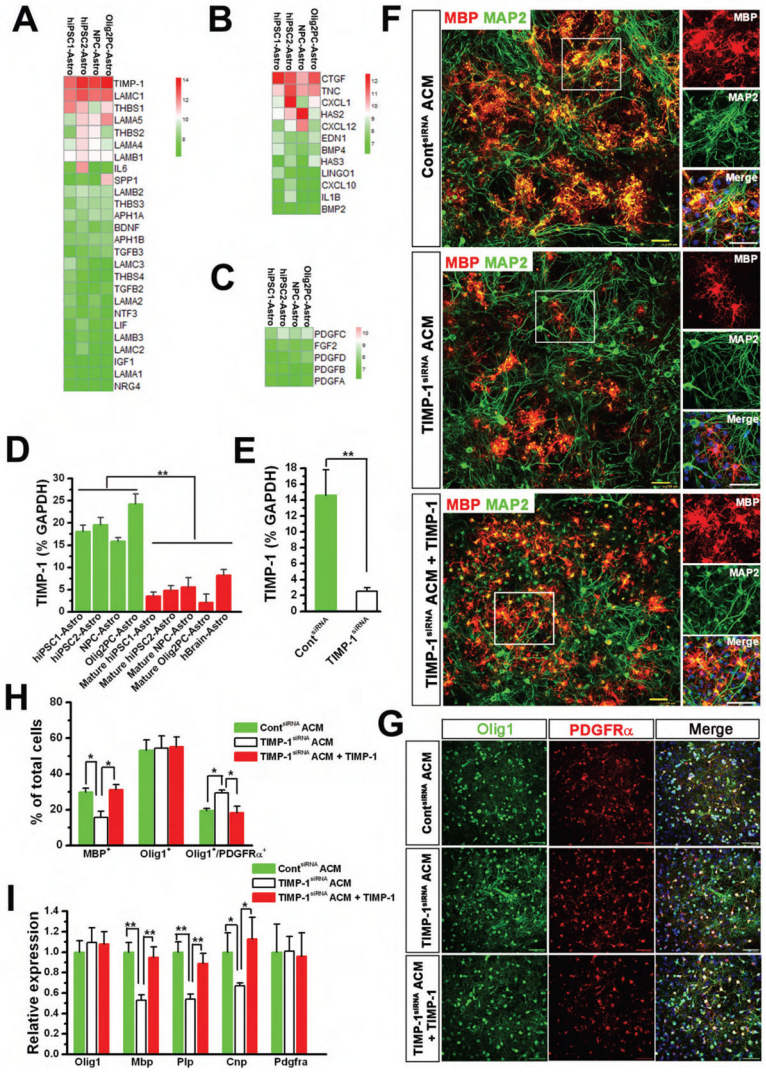


**Figure 4. The role of TIMP-1 in the effects of hiPSC-Astros on OPC differentiation**

**(A–C)** Gene expression analysis of immature hiPSC-Astros (hiPSC1-Astro and hiPSC2-Astro) and hESC-Astros (NPC-Astros and Olig2PC-Astros). Heat maps focusing on gene transcripts encoding factors that are secreted by astrocytes and are involved in promoting OPC differentiation (A), inhibiting OPC differentiation (B), and increasing OPC proliferation (C). High expressions relative to mean are colored red. Low expressions are colored green.

**(D)** qPCR analysis of *TIMP-1* expression in immature hiPSC-Astros and hESC-Astros, and in mature hiPSC-Astros, hESC-Astros and hBrain-Astros (n = 4 for each cell line). One-way ANOVA test, **P < 0.01.

**(E)** qPCR analysis of pooled data showing the expression of *TIMP-1* in hiPSC-Astros at 48 h after transfection with control (Cont) and *TIMP-1* siRNA (n = 3–5 from each line). Student's *t* test, **P < 0.01.

**(F)** Representatives of $MBP^+$ oligodendrocytes and $MAP2^+$ neurons in the primary mixed neuron/glia cultures fed with $Cont^{siRNA}$ ACM, TIMP-$1^{siRNA}$ ACM or TIMP-$1^{siRNA}$ ACM supplemented with TIMP-1. The squared areas are enlarged.

**(G)** Representatives of $Olig1^+$ and $PDGFR\alpha^+$ cells in the mix cultures fed with the different ACM.

**(H)** Quantification of pooled data showing the percentage of $MBP^+$, $Olig1^+$ and $Olig1^+$/$PDGFR\alpha^+$ cells in the cultures fed with the different ACM (n = 3 from each line). One-way ANOVA test, $^*P < 0.05$.

**(I)** qPCR analysis of pooled data showing *Olig1, Mbp, Plp, Cnp* and *Pdgfra* expression in the cultures fed with the different ACM (n = 3 from each line). One-way ANOVA test, $^*P < 0.05$ and $^{**}P < 0.01$. Scale bars, 50 μm. Blue, DAPI-stained nuclei.

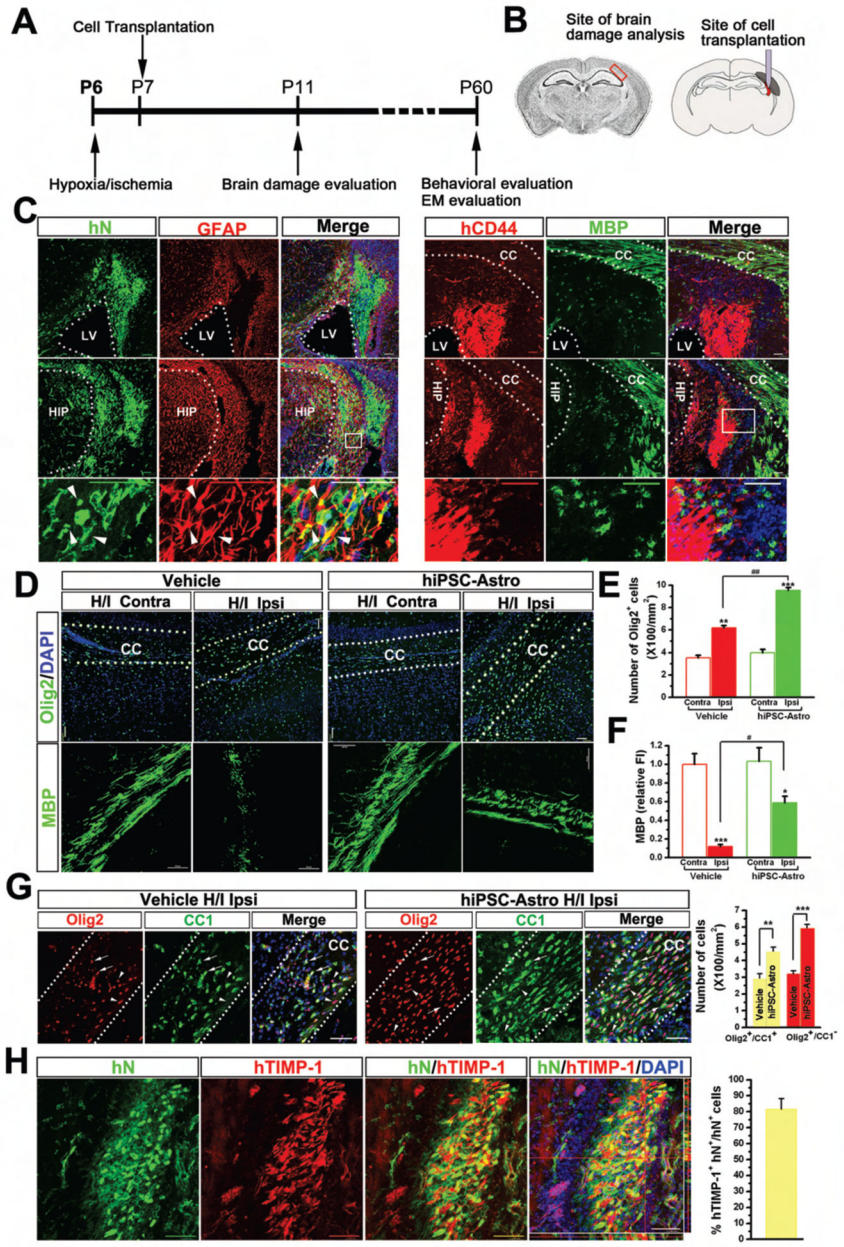


**Figure 5. Transplantation of immature hiPSC-Astros into *Rag1*−/− mouse brains subjected to PVL**

**(A)** A schematic diagram showing the timeline for the *in vivo* experiments from postnatal day (P) 6 to 60.

**(B)** *Left,* a cresyl violet-stained coronal brain section at the level of the hippocampus, where analyses occurred. The red box outlines the white matter area used for immunohistochemical analyses of PVL insult. *Right,* a diagram showing the cell transplantation site, which is adjacent to the injured white matter area.

**(C)** Representative images showing that grafted hiPSC-Astros are identified by human nuclei (hN) staining at P11. The transplanted hiPSC-Astros are also identified by hCD44,

but negative for MBP staining. The squared areas in the middle panels are enlarged in the bottom panels. Arrowheads indicate the $hN^+/GFAP^+$ cells. CC, corpus callosum; LV, lateral ventricle; and HIP, hippocampus.

**(D)** *Upper panels*, representative images showing that there are more $Olig2^+$ oligodendroglial cells in the ipsilateral (Ipsi) side than in the contralateral (Contra) side brain in both vehicle and hiPSC-Astro groups. Transplantation of hiPSC-Astros further increases the expansion of $Olig2^+$ cells in the Ipsi side. *Lower panels*, representative images showing that in vehicle group, MBP expression in the CC is only decreased substantially in the Ipsi side, with no significant changes in the Contra side. Transplantation of hiPSC-Astros promotes myelination in the Ipsi side and has no significant effect on the uninjured Contra side.

**(E)** The number of $Olig2^+$ cells in the analyzed area (n = 4 for each group). Student's *t* test, $^{**}P < 0.01$, and $^{***}P < 0.001$, comparison between the Ipsi side versus the Contra side; and $^{\#\#}P < 0.01$.

**(F)** Fluorescence intensity (FI) of MBP staining (n = 4 for each group). Data represent the FI value normalized to the Contra side brain of vehicle group. Student's *t* test, $^{*}P < 0.05$ and $^{***}P < 0.001$, comparison between Ipsi side versus Contra side; and $^{\#}P < 0.05$.

**(G)** Representatives and quantification of $Olig2^+/CC1^+$ and $Olig2^+/CC1^-$ cells in the Ipsi side brains of vehicle and hiPSC-Astro groups. Arrows indicate $Olig2^+/CC1^+$ cells and arrowheads indicate $Olig2^+/CC1^-$ cells. Student's *t* test, $^{**}P < 0.01$, and $^{***}P < 0.001$, n = 4 for each group.

**(H)** Representatives and quantification showing that the majority of $hN^+$ transplanted hiPSC-Astros are positive for human TIMP-1 (hTIMP-1) staining at P11. Scar bars, 50 μm. n = 4. Scale bars, 50 μm. Blue, DAPI-stained nuclei.

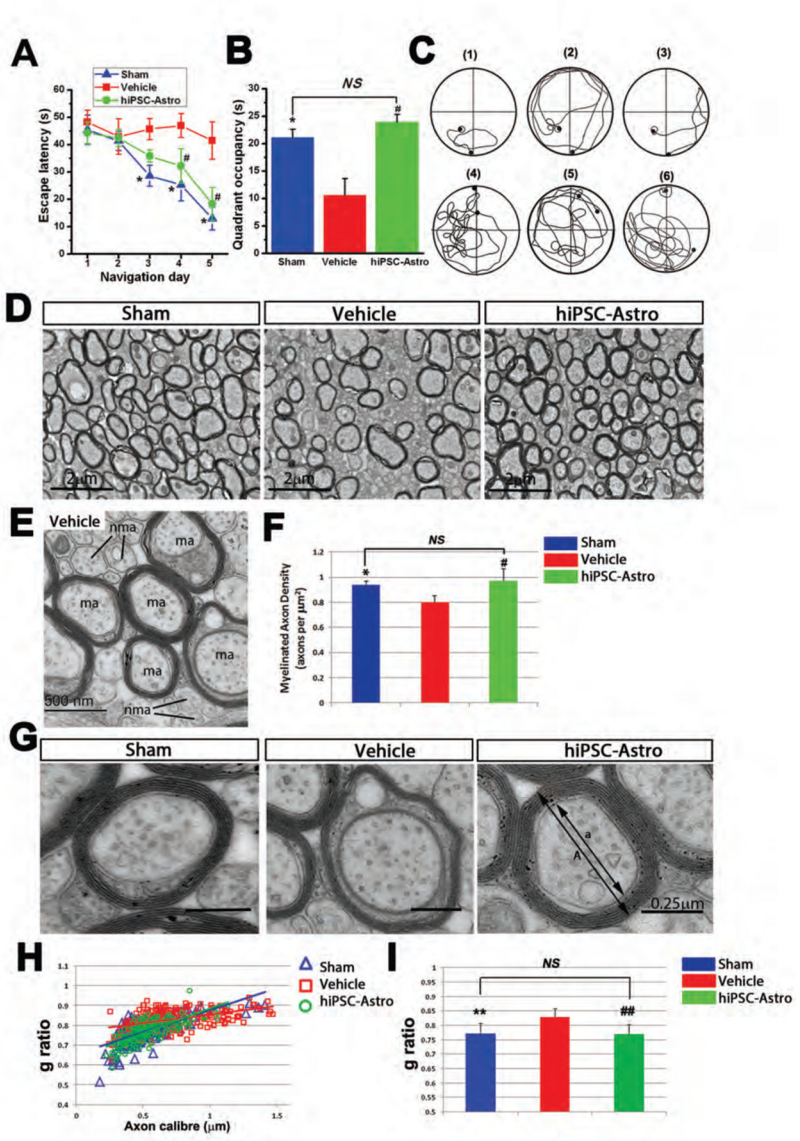


**Figure 6. The effects of transplanted immature hiPSC-Astros on behavioral recovery and myelin ultrastructure**

**(A)** Morris water-maze task is performed at P60 to test the spatial learning ability of sham (n = 7), vehicle (n = 8), and hiPSC-Astro (n = 10) transplanted groups, as shown by the time (escape latency) to find the submerged platform at navigation day 1 to 5. Two-way ANOVA test, *P < 0.05, comparison between vehicle group versus sham group; and #P < 0.05, comparison between vehicle group versus hiPSC-Astro group.

**(B)** Probe trials are performed 4 h after the last maze trails on navigation day 5, monitored by relative radial-quadrant occupancy (time spent in the target radial-quadrant) (n = 7 10). One way ANOVA test, *P < 0.05, comparison between vehicle group versus sham group; #P < 0.05, comparison between vehicle group versus hiPSC-Astro group; and *NS*, not significant.

**(C)** Representative sample paths from the maze trials ((1)–(3)) and the search patterns on the probe trials ((4)–(6)). (1),(4): sham group; (2),(5): vehicle group; (3),(6): hiPSC-Astro group.

**(D**) Low magnification electron micrographs showing a portion of corpus callosum from the animals in sham, vehicle and hiPSC-Astro groups. Scale bars, 2 μm.

**(E)** A enlarged image from vehicle group showing axons that have no compact myelin sheath (nma) among axons with myelin (ma). Scale bars, 500 nm.

**(F)** The density of myelinated axons of each group (n = 3 mice per group). One-way ANOVA test, *P < 0.05, comparison between vehicle group versus sham group; and # P < 0.05 comparison between vehicle group versus hiPSC-Astro group. *NS*, not significant.

**(G)** Representative electron micrographs in high magnification. Line “A” indicates diameter of a myelinated axon fiber and line “a” indicates diameter of axonal caliber. Scale bars, 0.25 μm.

**(H)** A scatter plot graph showing the relationship between g ratio values and axon diameters in the three groups (n = 3 mice per group).

**(I)** Mean g ratio of the three groups (n = 3 mice per group). One-way ANOVA test, **P < 0.01, comparison between vehicle group versus sham group; and $^{\#\#}$P < 0.01, comparison between vehicle group versus hiPSC-Astro group, and *NS*, not significant.

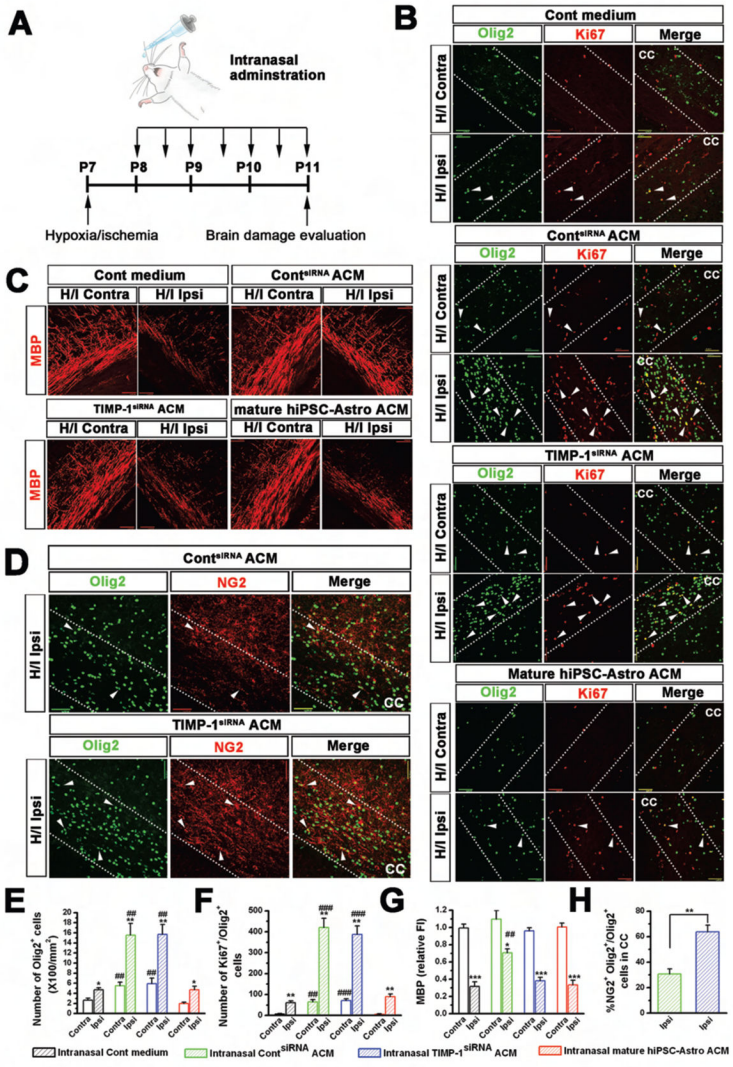


**Figure 7. Intranasal administration of ACM in a rat model of PVL**

**(A)** A schematic diagram showing the timeline for intranasal administration of ACM from P8 to P11.

**(B)** Representatives of $Olig2^+$ oligodendroglial cells and $Olig2^+/Ki67^+$ proliferating oligodendroglial cells, in Ipsi and Contra side brains from the rats received intranasal administration of control (Cont) medium, $Cont^{siRNA}$ ACM, $TIMP\text{-}1^{siRNA}$ ACM and mature hiPSC-Astro ACM. CC, corpus callosum. Arrowheads indicate the $Olig2^+/Ki67^+$ cells.

**(C)** Representatives of MBP expression in the CC of both Contra and Ipsi side brains from the four groups.

**(D)** Representatives of $Olig2^+$ and $NG2^+$ cells in the CC of the Ipsi side brains from $Cont^{siRNA}$ ACM and $TIMP\text{-}1^{siRNA}$ ACM groups. Arrowheads indicate the $Olig2^+/NG2^+$ cells.

**(E and F)** The number of $Olig2^+$ cells (E) and $Olig2^+/Ki67^+$ cells (F) in the analyzed area (n = 4 for each group). Student's *t* test, $^*P < 0.05$, and $^{***}P < 0.01$, comparison between Ipsi side versus Contra side within the different groups; and $^{\#\#}P < 0.01$ and $^{\#\#\#}P < 0.001$,

comparison between the Ipsi or Contra side from Cont medium group versus that from the other groups.

**(G)** Fluorescence intensity (FI) of MBP staining (n = 4 for each group). Data represent the FI value normalized to the Contra side brain of Cont medium group. Student's *t* test, *P < 0.05 and ***P < 0.001, comparison between Ipsi side versus Contra side within the different groups; and $^{\#\#}$P < 0.01, comparison between the Ipsi or Contra side from Cont medium group versus that from the other groups.

**(H)** The number of Olig2$^{+}$/NG2$^{+}$ cells in the CC of the Ipsi side brains from Cont$^{siRNA}$ ACM and TIMP-1$^{siRNA}$ ACM group (n = 4 for each group). Student's *t* test, **P < 0.01. Scar bars, 50 μm.